

Spectroscopy of the 1S_0 -to- 1D_2 clock transition in $^{176}\text{Lu}^+$

R. Kaewuam,¹ T. R. Tan,^{1,2} K. J. Arnold,¹ and M. D. Barrett^{1,2,*}

¹Centre for Quantum Technologies, National University of Singapore, 3 Science Drive 2, 117543 Singapore

²Department of Physics, National University of Singapore, 2 Science Drive 3, 117551 Singapore

(Dated: February 7, 2019)

High precision spectroscopy of the 1S_0 -to- 1D_2 clock transition of ^{176}Lu is reported. Measurements are performed with Hertz level precision with the accuracy of the hyperfine-averaged frequency limited by the calibration of an active hydrogen maser to the SI definition of the second via a GPS link. The measurements also provide accurate determination of the 1D_2 hyperfine structure. Hyperfine structure constants associated with the magnetic octupole and electric hexadecapole moments of the nucleus are considered, which includes a derivation of correction terms from third-order perturbation theory.

I. INTRODUCTION

Singly-ionized lutetium is a unique atomic clock candidate supporting three clock transitions: a highly forbidden magnetic dipole (M1) transition 1S_0 -to- 3D_1 at 848 nm, a spin-forbidden electric quadrupole (E2) transition 1S_0 -to- 3D_2 at 804 nm, and an E2 transition 1S_0 -to- 1D_2 at 577 nm. For each transition, hyperfine averaging eliminates shifts associated with the electronic angular momentum giving effective $J = 0$ levels with low sensitivity to electro-magnetic fields [1, 2]. Each transition has a unique sensitivity to environmental conditions such that frequency comparisons within the same apparatus provide important consistency checks for estimated systematic shifts.

Transitions at 848 and 804 nm have been observed [3, 4] and investigated [5], which demonstrated competitive properties with leading clock candidates. The 848-nm transition, in particular, offers an exceptionally low blackbody radiation (BBR) shift and all atomic properties relevant to clock performance offer an improvement over the Yb^+ octupole transition [2, 5]. Spectroscopy of the 577-nm transition has not yet been reported in the literature, but theoretical calculations [6] have recently been carried out indicating a BBR shift competitive with the quadrupole transitions in Sr^+ , Ca^+ , Hg^+ , and Yb^+ . Moreover, the calculated quadrupole moment of just $0.022 ea_0^2$ could be managed without the need for averaging.

In addition to clock applications, measuring the hyperfine structure of the long-lived 1D_2 level offers the possibility of extracting the relatively unexplored magnetic octupole and electric hexadecapole moments of the nucleus as for 3P_2 levels discussed in [7]. In that work only leading second-order corrections arising from the coupling to a neighbouring 3P_1 level were considered. Naively one might expect coupling to a singlet level to be diminished and hence the correction terms for the higher order nuclear moments minimal.

In this paper we report high-resolution measurements of the 1S_0 -to- 1D_2 optical transitions in $^{176}\text{Lu}^+$ from which we extract hyperfine splittings with Hertz level accuracy. Hyperfine structure constants associated with the nuclear magnetic octupole and electric hexadecapole moments are considered, which includes a derivation of correction terms up to third-order perturbation theory. Based on considerations for both 1D_2 and 3D_2 , it is argued that evidence of higher order multipole moments should include consideration of leading order corrections from this third-order extension. To our knowledge, such corrections have never been considered. The feasibility of conclusively observing the influence of the nuclear octupole and electric hexadecapole moments in $^{176}\text{Lu}^+$ is also discussed.

The paper is organized as follows. A description of the experimental system is given in section II, followed by the measurement procedures and results for 1D_2 in section III. Then, a brief summary of relevant hyperfine theory is given in section IV followed by its application to the 1D_2 and 3D_2 hyperfine structure in section V.

II. EXPERIMENTAL SETUP

Measurements are performed in a four-rod linear Paul trap with axial end-caps as described in [4]. Radial confinement is provided by a 16.8 MHz radio-frequency (rf) potential applied to a pair of diagonally opposing rods via a quarter-wave helical resonator, a small dc voltage applied to the other pair of rods ensures a splitting of the transverse frequencies, and the end caps are held at 8 V to provide axial confinement. In this configuration, the secular trapping frequencies are $(\omega_x, \omega_y, \omega_z) = 2\pi \times (610, 560, 130)$ kHz, with x, y indices denoting the two radial directions and z the trap axis. A magnetic field of ~ 0.24 mT defines a quantization axis.

The energy level structure of $^{176}\text{Lu}^+$ relevant to this work is shown in Fig. 1. There are three narrow linewidth optical transitions from the 1S_0 ground state to the upper 3D_1 , 3D_2 , and 1D_2 clock states. The lifetime of 3D_1 is estimated to be approximately 172 hours [3], and the lifetimes of 3D_2 and 1D_2 have been measured to be

* phybmd@nus.edu.sg

17.3 s and 180 ms respectively [8]. Doppler cooling and detection are achieved via scattering on the nearly closed 3D_1 -to- 3P_0 transition at 646 nm, which has a measured linewidth of $\sim 2\pi \times 2.45$ MHz [4, 9]. Optical pumping into 3D_1 is facilitated by driving the 1S_0 -to- 3P_1 , 3D_2 -to- 3P_1 , and 1D_2 -to- 3P_1 transitions at 350 nm, 622 nm, and 895 nm, respectively.

Spectroscopy of the 1D_2 level is implemented using a frequency-doubled extended-cavity-diode-laser system (ECDL) with a fundamental wavelength of 1154 nm. Second harmonic generation is accomplished using a fiberized, periodically-poled potassium titanyl phosphate (PPKTP) waveguide. The fundamental frequency is phase locked to an optical frequency comb (OFC). The short term (< 10 s) stability of the OFC is derived from a ~ 1 Hz linewidth laser at 848 nm which is referenced to a 10 cm long ultra-low expansion (ULE) cavity with finesse of $\sim 4 \times 10^5$. For longer times ($\gtrsim 10$ s), the OFC is steered to an active hydrogen maser (HM) reference. The frequency of the maser is calibrated to the SI (International System of Units) second by continuous comparison to a GPS timebase. The HM-GPS link exhibits a fractional instability of 2.8×10^{-14} /day. The 577-nm clock laser is switched with a double-passed acousto-optic modulator (AOM1 in in Fig. 2) which also controls the laser frequency relative to the comb. A schematic of the experimental setup is shown in Fig. 2.

III. MEASUREMENTS

Spectroscopy of the 1D_2 level follows a similar procedure to that reported in [4]. The atom is first optically pumped to 3D_1 with success checked in real time using a Bayesian detection scheme reported in [3]. When the atom is detected bright, the experiment continues with a 5 ms Doppler cooling pulse followed by optical pumping to $|{}^3D_1, F=7, m=0\rangle$. A π -pulse on the 848 nm clock transition is then applied to transfer the ion to $|{}^1S_0, 7, \pm 1\rangle$. The transfer efficiency of $\sim 95\%$ is limited by both state preparation of $|{}^3D_1, 7, 0\rangle$ and the clock π -pulse. The fidelity of population transfer is improved to better than 99.9% by state detection after the π -pulse. If the ion is detected bright, state preparation of $|{}^3D_1, 7, 0\rangle$ and shelving to $|{}^1S_0, 7, \pm 1\rangle$ is repeated. When a dark state is confirmed, the experiment proceeds with a π -polarized 577-nm clock pulse to drive a transition to the $|{}^1D_2, F', 0\rangle$ state, where $F' = 5, 6, \dots, 9$. Population remaining in 1S_0 is reshelled to 3D_1 with approximately 98% fidelity via a π -pulse from the 848-nm laser and subsequently detected by 646-nm fluorescence.

The transition probability when driving $|{}^1S_0, 7, +1\rangle$ to $|{}^1D_2, 6, 0\rangle$ as a function of either laser frequency offset or probe time is shown in Fig. 3. The limited coherence time indicated in Fig. 3(b) is likely limited by both the unstabilized ≈ 30 m optical fiber path from the laser source to the location of the ion and thermal dephasing. Nevertheless the 2 ms interrogation time provides sufficient

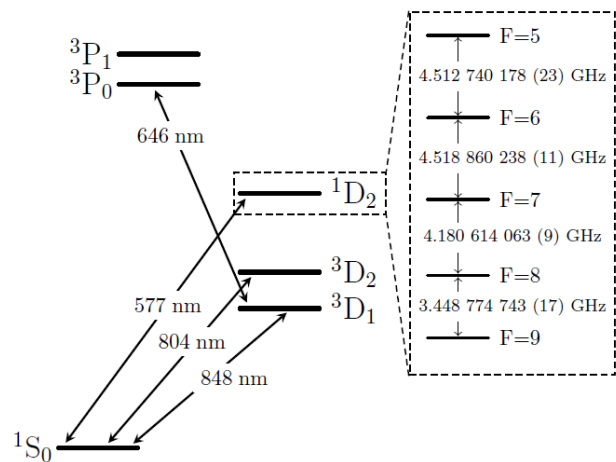


FIG. 1. Relevant energy level and transition diagram of a ${}^{176}\text{Lu}^+$ ion. The hyperfine interaction gives rise to five hyperfine levels in 1D_2 . The hyperfine splitting shown are determined from the measured transition frequencies of 1S_0 -to- 1D_2 . The uncertainties are the quadratic sum of statistical and systematic uncertainties.

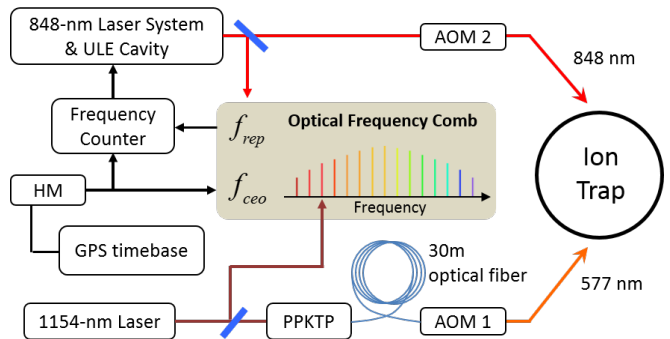


FIG. 2. Schematic diagram of the experiment. The optical frequency comb (OFC) is referenced to the 848-nm laser to stabilize f_{rep} and f_{ceo} is referenced to a HM. The 1154-nm laser is stabilized via phase locking to the OFC.

frequency resolution to resolve the ground state splitting.

To remove the first-order Zeeman shift of the ground state, the frequency of the 577-nm laser is steered to the average of a pair of Zeeman transitions from $|{}^1S_0, 7, \pm 1\rangle$ to $|{}^1D_2, F', 0\rangle$, using a servo technique similar to [10] that alternatively interrogates either side of each transition to derive error signals. There are four interrogations in total: two for $m_F = +1$ and two for $m_F = -1$. From these four points the laser frequency offset from the average transition frequency and splitting of two Zeeman components can be extracted. The appropriate error correction is applied to the oscillator driving AOM1 and recorded by a computer program. The servo to each of the hyperfine lines is implemented for a duration of ≈ 1000 s, and the corresponding statistical uncertainty of a measured optical frequency is at the ~ 1 Hz level limited by the flicker noise floor of the HM. The frequency offset

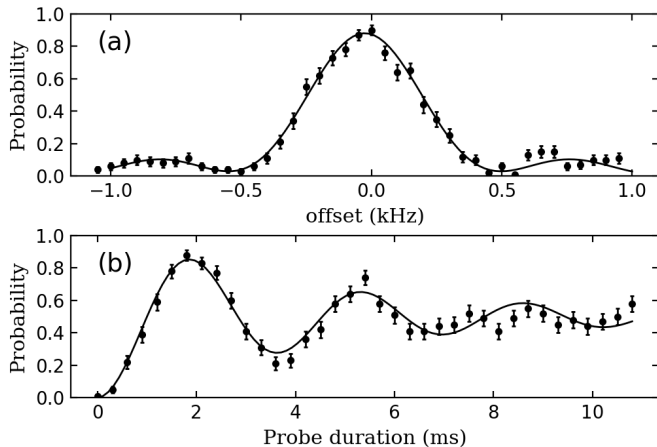


FIG. 3. Rabi spectroscopy of the transition from $|^1S_0, 7, +1\rangle$ to $|^1D_2, 6, 0\rangle$. Each point represents an average of 100 experiments. (a) Transition probability as a function of laser frequency offset for a fixed pulse time of 2 ms. (b) Rabi oscillation on the carrier transition. The model curve assumes dephasing of the oscillation due to thermal motion and an overall exponential damping, which accounts for the unstabilized optical fiber path.

and linear frequency drift of the HM were assessed by comparison with a GPS-linked reference over a 6 month period, yielding a fractional uncertainty of 3×10^{-15} of the HM frequency.

Interleaved with the 577-nm servo loop is a similar servo loop that steers the 848-nm laser to the average of transitions from $|^3D_1, 7, 0\rangle$ to $|^1S_0, 7, \pm 1\rangle$. This serves two purposes, (i) to determine the amplitude of the magnetic field from the difference of the two Zeeman transitions and (ii) provide a consistently check of the absolute frequency measurement methodology used for the 577-nm measurements. At each different 577-nm line measurement, which were taken over the course three days, the frequency of this 848-nm reference transition is measured from the interleaved servo. The systematic shifts affecting the 848-nm transition are expected to have instability well below the 1×10^{-15} level. The five reference measurements have an rms spread of 0.6 Hz, or 1.7×10^{-15} fractionally. This is consistent with statistical uncertainty of each measurement which is limited to 2×10^{-15} by the stability of the HM for a averaging time of 10^3 seconds. Additionally, a measurement of the 848-nm reference transition was repeated four months later and found to be in agreement at 2×10^{-15} (see Supplemental Material). This supports the 3×10^{-15} uncertainty assessment of the HM frequency from the GPS-link.

For the 1S_0 -to- 1D_2 transitions, systematic shifts at the Hz level are completely determined by quadratic Zeeman shifts: probe-induced ac-Stark shifts are negligibly small owing to the relatively short lifetime, the quadrupole moment for the 1D_2 is approximately two-orders of magnitude smaller than for the triplet states, and micromotion

is trivially controlled to the sub-Hz level. Expressions for the quadratic Zeeman shift are identical to those for the 3D_2 given in [4] differing only in the value of g_J . For convenience these expressions are given in Appendix A.

The Zeeman splitting between $|^1S_0, 7, \pm 1\rangle$ transitions is inferred from the 848-nm servo, to assess the strength of the magnetic field, B . As the laser couples both $m_F = \pm 1$ ground states to the upper $m'_F = 0$ state, the transition frequency of one Zeeman transition is shifted due to off-resonant coupling to the other Zeeman transition. The shifts are equal and opposite for the two transitions and thus do not lead to an overall shift in the Zeeman-averaged transition frequency. However, the accuracy in determining B can be degraded. With the interrogation time of ≈ 5 ms, the effect of off-resonant coupling is at the 0.1% level. This is much smaller than the accuracy of $g_I = -2.436 \times 10^{-4}$ [11, 12] of the 1S_0 level, which is assumed to be 0.5%. From the measured Zeeman splitting an average field of 0.2386(12) mT is deduced.

Within the LS-coupling limit, g_J for 1D_2 would be given by $g_L = 1$. Recent calculations have given $g_J = 1.01$ [6] indicating that mixing does not significantly influence the value. Consequently, we take the calculated value for g_J in determining the Zeeman shifts and assume the error is dominated by the magnetic field determined from the ground state. The resulting Zeeman-corrected optical frequencies, $\nu_{F'}$, for each of the transitions from $|^1S_0, 7, 0\rangle$ to $|^1D_2, F', 0\rangle$ are, in Hz units:

$$\nu_5 = 519\,622\,296\,515\,663.7 \pm (1.6)_{\text{stat}} \pm (31.2)_z, \quad (1a)$$

$$\nu_6 = 519\,617\,783\,775\,485.6 \pm (1.6)_{\text{stat}} \pm (8.5)_z, \quad (1b)$$

$$\nu_7 = 519\,613\,264\,915\,247.9 \pm (1.6)_{\text{stat}} \pm (2.1)_z, \quad (1c)$$

$$\nu_8 = 519\,609\,084\,301\,184.6 \pm (1.6)_{\text{stat}} \pm (10.4)_z, \quad (1d)$$

$$\nu_9 = 519\,605\,635\,526\,441.6 \pm (1.6)_{\text{stat}} \pm (27.3)_z, \quad (1e)$$

where the values in $(\dots)_{\text{stat}}$ denote statistical uncertainties in optical frequency measurement while $(\dots)_z$ are systematic uncertainties from the quadratic Zeeman shifts. As the systematic shifts arise from imperfect knowledge of the magnetic-field, they are strongly correlated. In particular the average frequency has a calculated magnetic field sensitivity of $1.2 \times 10^{-16}/\text{mT}^2$. Consequently, the average frequency here is limited completely by the statistical error.

IV. HYPERFINE INTERACTION THEORY

The accuracy of the measurements made allow high accuracy determination of hyperfine splittings, which are suitable for investigating hyperfine structure constants. For this purpose, we give a summary of relevant theory. We follow closely the work of Woodgate [13] and Bely [7], and include an extension to third order correction terms.

A nucleus can be approximately described as a point-like collection of electromagnetic moments. From the rel-

ativistic treatment in [7], the hyperfine Hamiltonian can be written as a sum of multipole interactions between electrons and nucleons,

$$H_{\text{hfs}} = \sum_{k=1}^{\infty} \mathbf{T}_{k,\mu}^e \cdot \mathbf{T}_k^n = \sum_{k=1}^{\infty} \sum_{\mu=-k}^k (-1)^\mu \mathbf{T}_{k,\mu}^e \mathbf{T}_{k,-\mu}^n, \quad (2)$$

where $\mathbf{T}_{k,\mu}^e$ and $\mathbf{T}_{k,\mu}^n$ are spherical tensor operators of rank k that operate on the space of electronic and nuclear coordinates, respectively. The sum excludes the term $k = 0$ because the monopole interaction is included in the unperturbed atomic Hamiltonian. Basis states where the total angular momentum $\mathbf{F} = \mathbf{I} + \mathbf{J}$ is conserved are denoted $|\gamma I J F m_F\rangle$ where γ denotes all other quantum numbers. From the Wigner-Eckart theorem, a matrix element of H_{hfs} over the basis set is,

$$\begin{aligned} \langle \gamma' I J F' m_F' | H_{\text{hfs}} | \gamma I J F m_F \rangle &= \delta_{FF'} \delta_{m_F' m_F} (-1)^{J'+I+F} \\ &\times \sum_{k=1}^{k'} \left\{ \begin{matrix} F & J' & I \\ k & I & J \end{matrix} \right\} \langle \gamma' J' || \mathbf{T}_k^e || \gamma J \rangle \langle I || \mathbf{T}_k^n || I \rangle, \quad (3) \end{aligned}$$

where $k' = \min(2I, J+J')$. Following the notations used in [13], the energy shift of a level with specific quantum numbers γ, J , and F can be expressed,

$$\begin{aligned} W_{JF} &= \sum_{k=1}^{k_m} X_k(IJF) U_k^{(1)}(J) \\ &+ \sum_{k=0}^{k_m} \left(X_k(IJF) \sum_{n=2}^{\infty} U_k^{(n)}(J) \right), \quad (4) \end{aligned}$$

where the F -dependent scale factor is given by,

$$X_k(IJF) = (-1)^{I+J+F} \frac{\left\{ \begin{matrix} F & J & I \\ k & I & J \end{matrix} \right\}}{\begin{pmatrix} I & k & I \\ -I & 0 & I \end{pmatrix} \begin{pmatrix} J & k & J \\ -J & 0 & J \end{pmatrix}}, \quad (5)$$

$k_m = \min(2I, 2J)$ is the minimum number of electromagnetic poles of either the relevant electronic state or the nucleus, and $U_k^{(n)}$ are terms arising from n^{th} -order perturbation theory. The form of Eq. 4 up to second-order was first derived by Woodgate [13]. Following that work, an outline of the derivation for $U_k^{(3)}(J)$ and the extension to all orders is given in Appendix B along with explicit expressions for $U_k^{(n)}$ up to $n = 3$.

Similar to the first-order correction, $X_k(IJF)$ appears as an overall multiplication factor for other perturbative corrections ($n > 1$), except the index k starts from $k = 0$ in the summation. Since $X_0(IJF) = 1$ for all possible quantum numbers F, J , and I , the energy shift is,

$$W_{JF} = \sum_{n=2}^{\infty} U_0^{(n)}(J) + \sum_{k=1}^{k_m} \sum_{n=1}^{\infty} X_k(IJF) U_k^{(n)}(J). \quad (6)$$

The first term in Eq. (6) implies an overall shift, which should properly be considered an isotope shift similar to the shifts arising from the finite size and finite mass of the nucleus [14]. To second order, this overall shift has been pointed out and discussed in [15]. The F -dependent factor $X_k(IJF)$ entering in the first- and second-order corrections in an identical way was first noted by Woodgate [13] and much later by Beloy and Derevianko [15]. Woodgate interpreted $U_k^{(2)}(J)$ as a second-order correction to $U_k^{(1)}(J)$, which has a direct relation to the conventional hyperfine constants A, B, C, \dots defined by,

$$A = \frac{1}{IJ} U_1^{(1)}(J), \quad (7a)$$

$$B = 4U_2^{(1)}(J), \quad (7b)$$

$$C = U_3^{(1)}(J), \quad (7c)$$

$$D = U_4^{(1)}(J). \quad (7d)$$

Notationally, it is convenient to introduce

$$U_k(J) = \sum_{n=1}^{\infty} U_k^{(n)}(J), \quad (8)$$

with $U_0^{(1)}(J) \equiv 0$. Equation 6 then has the simple form

$$W_{JF} = \sum_{k=0}^{k_m} X_k(IJF) U_k(J). \quad (9)$$

with the $k = 0$ term being a scalar, hyperfine-induced isotope shift. Hyperfine constants A', B', C', \dots related to $U_k(J)$ by equations analogous to Eqs. 7 can then be determined exactly from the hyperfine splittings. Throughout the literature A', B', \dots would be referred to as the uncorrected hyperfine structure constants with corrections made to accommodate the definitions given by Eqs 7.

V. HYPERFINE CONSTANTS OF 1D_2 AND 3D_2

Using the expressions given in Sec. IV, the energy shift W_F due to the hyperfine interaction for D_2 level in terms of (uncorrected) hyperfine constants can be readily determined. For both 1D_2 and 3D_2 , equations for the hyperfine splittings $\delta W_F = W_F - W_{F-1}$ are given by

$$\delta W_6 = 6A' - \frac{153}{364} B' + \frac{459}{91} C' - \frac{14535}{1001} D' \quad (10a)$$

$$\delta W_7 = 7A' - \frac{25}{104} B' - \frac{21}{13} C' + \frac{285}{13} D' \quad (10b)$$

$$\delta W_8 = 8A' + \frac{5}{91} B' - \frac{368}{91} C' - \frac{1520}{91} D' \quad (10c)$$

$$\delta W_9 = 9A' + \frac{27}{56} B' + \frac{27}{7} C' + \frac{45}{7} D' \quad (10d)$$

with the inverse relationships

$$A' = \frac{11}{525} \delta W_6 + \frac{51}{1400} \delta W_7 + \frac{117}{2800} \delta W_8 + \frac{19}{600} \delta W_9,$$

$$B' = -\frac{88}{105} \delta W_6 - \frac{5}{7} \delta W_7 + \frac{39}{238} \delta W_8 + \frac{247}{255} \delta W_9$$

$$C' = \frac{11}{150} \delta W_6 - \frac{7}{200} \delta W_7 - \frac{299}{3400} \delta W_8 + \frac{1729}{30600} \delta W_9$$

$$D' = -\frac{11}{1050} \delta W_6 + \frac{33}{1400} \delta W_7 - \frac{429}{23800} \delta W_8 + \frac{143}{30600} \delta W_9$$

From the measured optical frequencies given in Eq. (1), the uncorrected hyperfine constants for the 1D_2 level are, in Hz units,

$$A' = -543\,069\,419.3 \pm (1.7)_z \pm (0.07)_{\text{stat}} \quad (11a)$$

$$B' = 2\,984\,226\,871.4 \pm (8.8)_z \pm (2.8)_{\text{stat}} \quad (11b)$$

$$C' = 6\,904.2 \pm (1.5)_z \pm (0.3)_{\text{stat}} \quad (11c)$$

$$D' = -42.018 \pm (58)_z \pm (95)_{\text{stat}}. \quad (11d)$$

For comparison, using the optical frequencies measured in [4], the corresponding uncorrected hyperfine constants for the 3D_2 level are, in Hz units,

$$A' = 1\,370\,376\,728(8) \quad (12a)$$

$$B' = 1\,825\,831\,163(350) \quad (12b)$$

$$C' = 396\,959(42) \quad (12c)$$

$$D' = -1824(12). \quad (12d)$$

The value of D' for 3D_2 is slightly different than that reported in [4] owing to an incorrect g_J factor used in the evaluation of Zeeman shifts. Appropriately corrected optical frequencies are tabulated in Appendix A.

It should be noted that there is a large cancellation of systematic shifts in the determination of these coefficients. The D' coefficient in particular has a Zeeman dependence of just -180 Hz/mT^2 and 100 Hz/mT^2 for 3D_2 and 1D_2 respectively. Consequently the statistical errors can be significant even if the quadratic Zeeman shift systematic dominates the frequency uncertainty. Statistical errors are much larger for the 3D_2 measurements owing to the stability of the optical comb used at that time.

To compare these values to the usual hyperfine constants proportional to the appropriate electromagnetic moment of the nucleus, correction terms must be calculated. As noted in [15], leading order dipole-dipole (d-d), and dipole-quadrupole (d-q) corrections do not contribute to D and only d-q corrections apply to C . This has been proved as special cases in [7, 16], but the general second-order correction derived by Woodgate [13] and given in Eq. B2 makes this immediate from the 6-j symbols involved.

Including only d-q corrections, the corrected C coefficient for the 1D_2 level is given by

$$C = C' + \zeta(^3D_1) - \sqrt{\frac{3}{7}}\zeta(^3D_2) + \frac{1}{7}\sqrt{\frac{3}{2}}\zeta(^3D_3), \quad (13)$$

where

$$\zeta(^3D_J) = \frac{6}{175}\mu Q \frac{\langle ^3D_J || \mathbf{T}_1^e || ^1D_2 \rangle \langle ^3D_J || \mathbf{T}_2^e || ^1D_2 \rangle}{E_{^1D_2} - E_{^3D_J}}, \quad (14)$$

with μ and Q being the usual magnetic dipole and electric quadrupole moment of the nucleus respectively. A similar expression can be found for the 3D_2 level by interchanging 1D_2 and 3D_2 in all expressions.

Matrix elements for these corrections are not available for all contributions. However, matrix elements for contributions from 3D_1 have been computed for the purposes

of estimating hyperfine quenching rates of the 3P_0 level used for state detection [8]. Relevant values are tabulated in Table I. In the case of the 3D_2 level these give a correction of approx 360(100) kHz, which has the same sign and magnitude of C' . As other terms have a larger energy denominator and smaller coefficient in Eq. 13, we would not expect these to provide a large cancellation indicating a fairly large value for C . For the 1D_2 level, the corresponding contribution from 3D_1 is $\sim -2.4\text{ kHz}$ with an error bar of 50%. This has the opposite sign as C' so leads to a some cancellation. Thus it would appear there is likely a very large difference in the C coefficient for the triplet and singlet $J = 2$ levels.

TABLE I. Matrix elements of the electronic operators \mathbf{T}_1^e and \mathbf{T}_2^e in units of MHz/ μ_N and MHz/barn, respectively. Values are taken from [8]^a. Note that signs of the matrix elements depend on a convention choice but relative signs between them are fixed by that choice.

ME	Value
$\langle ^3D_1 \mathbf{T}_1^e ^1D_2 \rangle$	-10620 (870)
$\langle ^3D_1 \mathbf{T}_2^e ^1D_2 \rangle$	70 (45)
$\langle ^3D_1 \mathbf{T}_1^e ^3D_2 \rangle$	18680 (1900)
$\langle ^3D_1 \mathbf{T}_2^e ^3D_2 \rangle$	700 (100)
$\langle ^3D_1 \mathbf{T}_2^e ^3D_3 \rangle$	200 (50)

^a Signs were not given [8] and one matrix element was missing. These were given in a private communication.

For the D coefficient, leading second-order corrections are q-q and possibly dipole-octupole (d-o). Including only these terms the expression for the 1D_2 level is given by

$$D = D' + \xi(^3D_1) - \frac{3}{7}\xi(^3D_2) + \frac{3}{28}\xi(^3D_3) - \chi(^3D_1) + \frac{1}{\sqrt{6}}\chi(^3D_2) - \frac{1}{3\sqrt{14}}\chi(^3D_3), \quad (15)$$

where

$$\xi(^3D_J) = \frac{33}{15925}Q^2 \frac{|\langle ^3D_J || \mathbf{T}_2^e || ^1D_2 \rangle|^2}{E_{^1D_2} - E_{^3D_J}}, \quad (16)$$

and

$$\chi(^3D_J) = \frac{11}{245}\sqrt{\frac{2}{7}}\mu\Omega \times \frac{\langle ^3D_J || \mathbf{T}_1^e || ^1D_2 \rangle \langle ^3D_J || \mathbf{T}_3^e || ^1D_2 \rangle}{E_{^1D_2} - E_{^3D_J}}. \quad (17)$$

with Ω the magnetic octupole moment of the nucleus as defined in [7]. Expressions for 3D_2 can again be obtained by interchanging 1D_2 and 3D_2 .

Only $\xi(^3D_1)$ can be estimated from the given matrix elements giving $\sim 1280(430)\text{ Hz}$ and $\sim 1.5\text{ Hz}$ for the 3D_2 and 1D_2 levels, respectively. The correction for 1D_2 is only accurate to about a factor of 3 but is clearly much

smaller than D' in this case. Since $\xi(^3D_J)$ is positive definite there will be some cancellation of other q-q corrections, but it is unclear if d-o corrections would contribute significantly.

Leading third order corrections for the D coefficient would be d-d-q corrections and these should not be disregarded. As a crude estimate, such terms would have the scale of a d-q correction term for C multiplied by the ratio of a T_1^e matrix element and an energy separation. Including the magnetic dipole moment, the matrix element is on the order 10 GHz and energy separations are on the order of 10 THz. Hence, we might expect d-d-q corrections to be on the order of 10^{-3} of the d-q corrections for C . For both 1D_2 and 3D_2 these would be of similar magnitude to the estimated q-q corrections for the respective D coefficient. For the same reasons, d-d-d corrections to C may also be important. To our knowledge, third order corrections have never been considered.

Even if all required matrix elements were calculated, evidence of the higher order multipole moments would be contingent on the validity of those calculations and, ideally, that validity should be experimentally tested. Since the matrix elements essentially determine a hyperfine mixing between fine-structure levels, any measurable consequence of that mixing could serve as a test of the theory. For Lu^+ , such mixing would give rise to: (a) decays from 3P_0 to levels other than 3D_1 , (b) deviations of the g -factors applicable to the upper state and (c) forbidden transitions from the ground-state such as E2 transitions to 3D_1 or M1 transitions to 1D_2 or 3D_2 . Measured rates for quenching decays from 3P_0 in $^{175}\text{Lu}^+$ were reported in [8]. Quadrupole transitions from 3D_1 to 1S_0 have also been observed and coupling strengths could be readily calibrated. Ultimately it is desirable to have high precision measurements of g -factors for the assessment of magnetic fields and the average of g_F over all hyperfine levels is g_I [1]. Thus, there is opportunity to rigorously test the accuracy of correction terms.

VI. SUMMARY

In this paper we have performed high resolution spectroscopy of the 1S_0 -to- 1D_2 clock transition in $^{176}\text{Lu}^+$. Transitions to all hyperfine levels have been measured to Hertz level precision. This sets the stage for clock operation incorporating hyperfine averaging in which the laser is servoed over all five transitions measured here. Limited knowledge of g_I limits the current accuracy of individual transitions but this uncertainty can be significantly reduced with improved assessment of g_I . Moreover, hyperfine averaging practically eliminates the systematic uncertainty associated with the static magnetic field. As a by-product of this work we have extracted accurate determinations of the hyperfine structure.

Having accurate assessments of the hyperfine splittings for 1D_2 and 3D_2 prompted us to investigate the possible influence of higher order nuclear moments, specif-

ically the magnetic octupole and electric hexadecapole moment. To this end we have extended previous theory work to include third order perturbation theory. We have argued that proper analysis of the higher-order nuclear moments should consider at least the leading order terms that appear in the third-order result.

In the case of $^{176}\text{Lu}^+$, it is unclear if theory could attain sufficient accuracy to allow conclusive confirmation on the existence of the higher order nuclear moments, but experiments have been suggested that could at least test the validity of theoretical results. Similar such experiments would be applicable in any system claiming to have observed these properties. In the case of $^{176}\text{Lu}^+$, the experimental tests would be readily accessible as the system is developed towards a high performance clock.

ACKNOWLEDGMENTS

We thank Vladimir Dzuba, Marianna Safronova and Sergey Porsev for useful discussions. This work is supported by the National Research Foundation, Prime Ministers Office, Singapore and the Ministry of Education, Singapore under the Research Centres of Excellence programme. This work is also supported by A*STAR SERC 2015 Public Sector Research Funding (PSF) Grant (SERC Project No: 1521200080). T. R. Tan acknowledges support from the Lee Kuan Yew post-doctoral fellowship.

Appendix A: Quadratic Zeeman shifts.

Expressions for the quadratic Zeeman shifts for both the 1D_2 and 3D_2 are functionally equivalent differing only in the value of g_J and the hyperfine splittings. Defining the hyperfine interval $\delta\nu_{F'} = \nu_{F'} - \nu_{F'-1}$ in units of frequency, the quadratic shifts $\Delta_{F'}$ for the $m_{F'} = 0$ states are:

$$\Delta E_5/h = -\frac{16}{13} \frac{\mathcal{R}}{\delta\nu_6}, \quad (\text{A1a})$$

$$\Delta E_6/h = \frac{16}{13} \frac{\mathcal{R}}{\delta\nu_6} - \frac{102}{65} \frac{\mathcal{R}}{\delta\nu_7}, \quad (\text{A1b})$$

$$\Delta E_7/h = \frac{102}{65} \frac{\mathcal{R}}{\delta\nu_7} - \frac{117}{85} \frac{\mathcal{R}}{\delta\nu_8}, \quad (\text{A1c})$$

$$\Delta E_8/h = \frac{117}{85} \frac{\mathcal{R}}{\delta\nu_8} - \frac{14}{17} \frac{\mathcal{R}}{\delta\nu_9}, \quad (\text{A1d})$$

$$\Delta E_9/h = \frac{14}{17} \frac{\mathcal{R}}{\delta\nu_9}. \quad (\text{A1e})$$

where $\mathcal{R} = (g_J - g_I)^2 \mu_B^2 B^2 / h^2$ with g_J and g_I the usual g -factors. Within the LS-coupling limit $g_J = 1$ and $7/6$ for 1D_2 and 3D_2 , respectively.

In [4], the calculated Zeeman shifts inadvertently used a value of $g_J = 1/2$. The appropriately corrected optical

frequencies are, in Hz,

$$\nu_5 = 372\,776\,905\,829\,552 \text{ (200)}, \quad (\text{A2a})$$

$$\nu_6 = 372\,784\,362\,667\,641 \text{ (200)}, \quad (\text{A2b})$$

$$\nu_7 = 372\,793\,515\,721\,790 \text{ (200)}, \quad (\text{A2c})$$

$$\nu_8 = 372\,804\,577\,481\,195 \text{ (200)}, \quad (\text{A2d})$$

$$\nu_9 = 372\,817\,792\,702\,607 \text{ (200)}. \quad (\text{A2e})$$

Appendix B: Third-order hyperfine corrections

In this section an outline of the third-order correction to the HFS is given illustrating that it has the same F -dependent factor $X_k(IJF)$ as the first- and second-order terms. The derivation illustrates how the form of the perturbation can be extended to all orders of perturbation theory. For completeness, expressions for the first- and second-order terms are also given, which also establishes notation.

Using the notation $\mathcal{I}^{(k)} \equiv \langle I || \mathbf{T}_k^n || I \rangle$ and $\mathcal{Q}_{J_1 J_2}^{(k)} \equiv \langle J_1 || \mathbf{T}_k^e || J_2 \rangle$ for the reduced nuclear and electronic matrix elements, respectively, expressions for $U_k^{(1)}(J)$ and

$U_k^{(2)}$ are given by [13],

$$U_k^{(1)}(J) = \begin{pmatrix} I & k & I \\ -I & 0 & I \end{pmatrix} \begin{pmatrix} J & k & J \\ -J & 0 & J \end{pmatrix} \mathcal{I}^{(k)} \mathcal{Q}_{JJ}^{(k)}, \quad (\text{B1})$$

and

$$U_k^{(2)}(J) = \begin{pmatrix} I & k & I \\ -I & 0 & I \end{pmatrix} \begin{pmatrix} J & k & J \\ -J & 0 & J \end{pmatrix} \\ \times \sum_{k_1 k_2} \left[(-1)^{2I+2J+k_1+k_2+k} (2k+1) \right. \\ \times \left. \begin{Bmatrix} k_1 & k_2 & k \\ I & I & I \end{Bmatrix} \mathcal{I}^{(k_1)} \mathcal{I}^{(k_2)} \right. \\ \left. \times \sum_{J'} \left\{ \begin{Bmatrix} k_1 & k_2 & k \\ J & J & J' \end{Bmatrix} \frac{\mathcal{Q}_{JJ'}^{(k_1)} \mathcal{Q}_{J'J}^{(k_2)}}{(E_J - E_{J'})} \right\} \right], \quad (\text{B2})$$

respectively, where E_J is the unperturbed fine-structure energy.

Using Eq. (3), the third-order correction to the energy W_{JF} can be written in the compact form

$$W_{JF}^{(3)} = \sum_{J' J''} \frac{\mathcal{P} - \mathcal{G}}{(E_J - E_{J'})(E_J - E_{J''})}, \quad (\text{B3})$$

where \mathcal{P} and \mathcal{G} are given by

$$\mathcal{P} = \sum_{k_1 k_2 k_3} (-1)^{3I+J+J'+J''+3F} \begin{Bmatrix} F & J & I \\ k_1 & I & J' \end{Bmatrix} \begin{Bmatrix} F & J' & I \\ k_2 & I & J'' \end{Bmatrix} \begin{Bmatrix} F & J'' & I \\ k_3 & I & J \end{Bmatrix} \mathcal{I}^{(k_1)} \mathcal{I}^{(k_2)} \mathcal{I}^{(k_3)} \mathcal{Q}_{JJ'}^{(k_1)} \mathcal{Q}_{J'J''}^{(k_2)} \mathcal{Q}_{J''J}^{(k_3)} \quad (\text{B4a})$$

$$\mathcal{G} = \delta_{J' J''} \sum_{k_1 k_2 k_3} (-1)^{3I+2J+J'+3F} \begin{Bmatrix} F & J & I \\ k_1 & I & J \end{Bmatrix} \begin{Bmatrix} F & J & I \\ k_2 & I & J' \end{Bmatrix} \begin{Bmatrix} F & J' & I \\ k_3 & I & J \end{Bmatrix} \mathcal{I}^{(k_1)} \mathcal{I}^{(k_2)} \mathcal{I}^{(k_3)} \mathcal{Q}_{JJ}^{(k_1)} \mathcal{Q}_{JJ'}^{(k_2)} \mathcal{Q}_{J'J}^{(k_3)}. \quad (\text{B4b})$$

Following Woodgate [13], the *Biedenharn-Elliott* identity [17, pg 305, Eq. 7] can be used to reduce the number of 6j-symbols having an F dependence. Explicitly, the last two 6j-symbols in Eq. B4a can be written

$$(-1)^{J+J'+J''+3I+F} \begin{Bmatrix} J' & I & F \\ I & J'' & k_2 \end{Bmatrix} \begin{Bmatrix} J & I & F \\ I & J'' & k_3 \end{Bmatrix} = \sum_K (-1)^{k_2+k_3+K} (2K+1) \begin{Bmatrix} J' & J & K \\ I & I & F \end{Bmatrix} \begin{Bmatrix} k_2 & k_3 & K \\ J & J' & J'' \end{Bmatrix} \begin{Bmatrix} k_2 & k_3 & K \\ I & I & I \end{Bmatrix}.$$

This increases the number of 6j-symbols in Eq. B4a by one but reduces the number with an F -dependence to just two. Applying the identity again reduces this to just one, which is exactly the factor required for Eq. 4. Treating Eq. B4b in a similar way provides the desired expansion with $U_k^{(3)}(J)$ given by

$$U_k^{(3)}(J) = \begin{pmatrix} I & k & I \\ -I & 0 & I \end{pmatrix} \begin{pmatrix} J & k & J \\ -J & 0 & J \end{pmatrix} \sum_{J' J''} \frac{(2k+1)}{(E_J - E_{J'})(E_J - E_{J''})} \sum_{k_1 k_2 k_3} \sum_K (-1)^{2K+\alpha} (2K+1) \\ \times \left[(-1)^{J-J''} \begin{Bmatrix} k_1 & J & J' \\ J & K & k \end{Bmatrix} \begin{Bmatrix} k_1 & I & I \\ I & K & k \end{Bmatrix} \begin{Bmatrix} k_2 & J' & J'' \\ J & k_3 & K \end{Bmatrix} \begin{Bmatrix} k_2 & k_3 & K \\ I & I & I \end{Bmatrix} \mathcal{I}^{(k_1)} \mathcal{I}^{(k_2)} \mathcal{I}^{(k_3)} \mathcal{Q}_{JJ'}^{(k_1)} \mathcal{Q}_{J'J''}^{(k_2)} \mathcal{Q}_{J''J}^{(k_3)} \right. \\ \left. - \delta_{J' J''} \begin{Bmatrix} k_1 & J & J \end{Bmatrix} \begin{Bmatrix} k_1 & I & I \\ I & K & k \end{Bmatrix} \begin{Bmatrix} k_2 & J & J' \\ J & k_3 & K \end{Bmatrix} \begin{Bmatrix} k_2 & k_3 & K \\ I & I & I \end{Bmatrix} \mathcal{I}^{(k_1)} \mathcal{I}^{(k_2)} \mathcal{I}^{(k_3)} \mathcal{Q}_{JJ}^{(k_1)} \mathcal{Q}_{JJ'}^{(k_2)} \mathcal{Q}_{J'J}^{(k_3)} \right], \quad (\text{B5})$$

where $\alpha = 3J' + 3J'' + 2J + k + k_1 + k_2 + k_3$. The summation of the 6j-symbols over K can be conveniently written

in terms of a 12j-symbol of the second kind [17, pg 367] to give

$$U_k^{(3)}(J) = \begin{pmatrix} I & k & I \\ -I & 0 & I \end{pmatrix} \begin{pmatrix} J & k & J \\ -J & 0 & J \end{pmatrix} \sum_{\substack{J', J'' \\ k_1 k_2 k_3}} \frac{(-1)^\alpha (2k+1)}{(E_J - E_{J'})(E_J - E_{J''})} \\ \times \left[\begin{pmatrix} - & J & k_3 & J'' \\ I & - & I & k_2 \\ k_1 & J & - & J' \\ I & k & I & - \end{pmatrix} \mathcal{Q}_{JJ'}^{(k_1)} \mathcal{Q}_{J'J''}^{(k_2)} \mathcal{Q}_{J''J}^{(k_3)} - \delta_{J'J''} (-1)^{J'-J} \begin{pmatrix} - & J & k_3 & J' \\ I & - & I & k_2 \\ k_1 & J & - & J \\ I & k & I & - \end{pmatrix} \mathcal{Q}_{JJ}^{(k_1)} \mathcal{Q}_{JJ'}^{(k_2)} \mathcal{Q}_{J'J}^{(k_3)} \right] \mathcal{I}^{(k_1)} \mathcal{I}^{(k_2)} \mathcal{I}^{(k_3)}. \quad (\text{B6})$$

In this form, properties of the 12j-symbol make it immediately clear that $k \leq k_1 + k_2 + k_3$ for a non-zero contribution.

The validity of the form of the perturbation to any order can be established by induction. For n^{th} -order perturbation theory, the most general term has 6j-symbols appearing in the form

$$\left\{ \begin{matrix} F & J & I \\ k_1 & I & J^{(1)} \end{matrix} \right\} \\ \times \left(\left\{ \begin{matrix} F & J^{(n-1)} & I \\ k_n & I & J \end{matrix} \right\} \prod_{j=2}^{n-1} \left\{ \begin{matrix} F & J^{(j-1)} & I \\ k_j & I & J^{(j)} \end{matrix} \right\} \right), \quad (\text{B7})$$

with all others as a special case, just as \mathcal{G} is a special case of \mathcal{P} in third-order perturbation. If it is assumed the term in parentheses can be reduced to a product of 6j-symbols with only one having an F-dependence given by

$$\left\{ \begin{matrix} F & J^{(1)} & I \\ K & I & J \end{matrix} \right\}, \quad (\text{B8})$$

the *Biedenharn-Elliott* identity can be used to produce same F -dependent factor as the first order result. Moreover, the same identity can also be used to inductively infer the validity the assumption to any order.

-
- [1] M. D. Barrett. Developing a field independent frequency reference. *New J. Phys.*, 17:053024, 2015.
- [2] HCJ Gan, G Maslennikov, K-W Tseng, TR Tan, R Kaewuam, KJ Arnold, D Matsukevich, and MD Barrett. Oscillating-magnetic-field effects in high-precision metrology. *Physical Review A*, 98(3):032514, 2018.
- [3] K. J. Arnold, R. Kaewuam, A. Roy, E. Paez, S. Wang, and M. D. Barrett. Observation of the 1S_0 to 3D_1 clock transition in $^{175}\text{Lu}^+$. *Phys. Rev. A*, 94:052512, 2016.
- [4] R. Kaewuam, A. Roy, T. R. Tan, K. J. Arnold, and M. D. Barrett. Laser spectroscopy of $^{176}\text{Lu}^+$. *J. Mod. Opt.*, 65:592, 2017.
- [5] K. J. Arnold, R. Kaewuam, A. Roy, T. R. Tan, and M. D. Barrett. Blackbody radiation shift assessment for a lutetium ion clock. *Nature Communications*, 9:1650, 2018.
- [6] SG Porsev, UI Safronova, and MS Safronova. Clock-related properties of Lu^+ . *arXiv preprint arXiv:1806.02909*, 2018.
- [7] K. Beloy, A. Derevianko, and W. R. Johnson. Hyperfine structure of the metastable 3P_2 state of alkaline-earth-metal atoms as an accurate probe of nuclear magnetic octupole moments. *Phys. Rev. A*, 77:012512, 2008.
- [8] E. Paez, K. J. Arnold, E. Hajiyev, S. G. Porsev, V. A. Dzuba, U. I. Safronova, M. S. Safronova, and M. D. Barrett. Atomic properties of Lu^+ . *Phys. Rev. A*, 93:042112, 2016.
- [9] K. J. Arnold, R. Kaewuam, T. R. Tan, S. G. Porsev, M. S. Safronova, and M. D. Barrett. Dynamic polarizability measurements in $^{176}\text{Lu}^+$. *arXiv preprint arXiv:1810.11168*, 2018.
- [10] J.E. Bernard, L. Marmet, and A. A. Madej. A laser frequency lock referenced to a single trapped ion. *Opt. Commun.*, 150:170, 1998.
- [11] George J Ritter. Hyperfine structure and nuclear moments of ^{175}Lu . *Phys. Rev.*, 126:240, 1962.
- [12] T. Brenner, S. Buttgenbach, W. Rupprecht, and F. Traber. Nuclear moments of the low abundant natural isotope ^{176}Lu and hyperfine anomalies in the lutetium isotopes. *Nucl. Phys. A*, 440:407, 1985.
- [13] GK Woodgate. Hyperfine structure and nuclear moments of samarium. *Proc. R. Soc. Lond. A*, 293(1432):117-144, 1966.
- [14] W. H. King. *Isotope shifts in atomic spectra*. Springer, New York, 1984.
- [15] K. Beloy and A. Derevianko. Second-order effects on the hyperfine structure of p states of alkali-metal atoms. *Phys. Rev. A*, 78:032519, 2008.
- [16] K Beloy, A Derevianko, VA Dzuba, GT Howell, BB Blinov, and EN Fortson. Nuclear magnetic octupole moment and the hyperfine structure of the $^5D_{3/2,5/2}$ states of the Ba^+ ion. *Physical Review A*, 77(5):052503, 2008.
- [17] D. A. Varshalovich, A. N. Moskalev, and V. K. Khersonskii. *Quantum theory of angular momentum*. World Scientific, 1988.